# Chapter 17
# The Drag Build-up Method

## 17.1 Description

A way of making an estimate of the drag area is to model the car as a composite of shape elements which have known drag coefficients. The drag areas of these shape elements are added to give the drag area of the car at a particular speed. This is called the *drag build-up* method.

Figure 17.1 shows two views of a solar car. An arrow representing the drag of each shape element is shown attached to that element. The front view shows the profile areas of each element. The profile area of the car is the sum of the element profile areas; likewise, the total drag force is the sum of the element drag forces. But each element drag force can be represented by Eq. (2.1), and dividing out the dynamic pressure, $q$, which is the common factor, gives an equation for the drag area of the composite shape. Therefore, if there are $n_E$ shape elements, the drag area estimate would be, including ventilation drag,

$$c_D A_D = \sum_{i=1}^{i=n_E} (c_D A_D)_i + c_V A_D. \tag{17.1}$$

Both viscous friction and separation are included in the drag coefficient measurements of the individual shape elements. Chapter 18 explains how to estimate the ventilation drag, represented by $c_V$ in Eq. (17.1).

**Corrections** When shapes are assembled into a car or brought near the ground, their drag contributions are altered by the change in the airflow caused by the nearness of the other shapes or the ground. Also, the surface of an actual car will usually be rougher than that of a more idealized mathematical model and the smoothed shape elements tested in wind tunnels.

Furthermore, objects such as rearview mirrors and antennas must be attached to some of the shape elements. The drag contributed by these protuberances must also be included.



E. F. Thacher, *A Solar Car Primer,* DOI 10.1007/978-3-319-17494-5_17

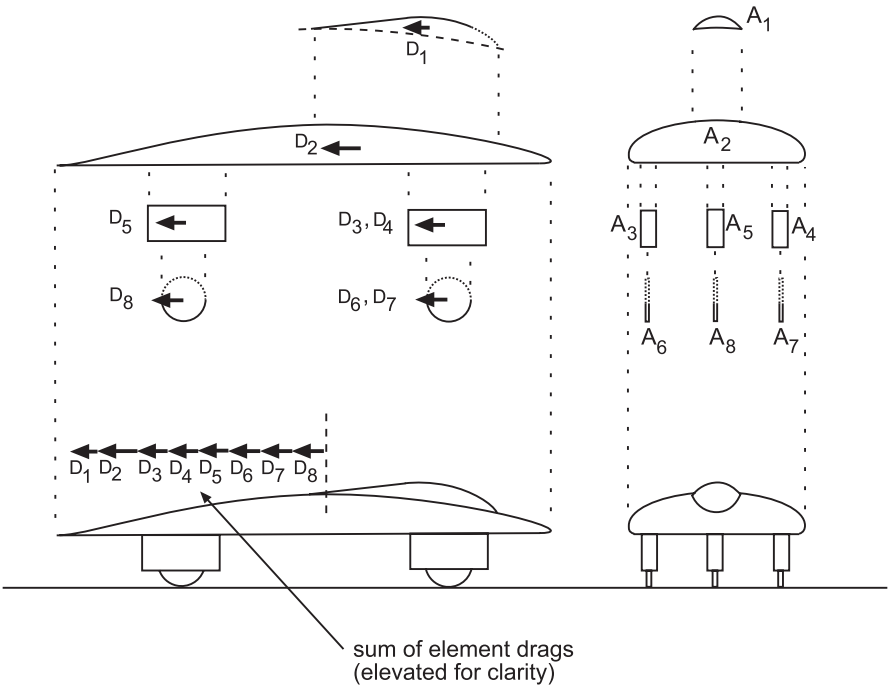


**Fig. 17.1** Drag elements

The drag measurement of a shape element that has been taken free of the influence of the other elements, the ground, the roughness that comes from fabrication, and protuberances is called a *free air* measurement. It is denoted by $c_{D\infty}$. Corrections for interference, ground effect, protuberance, and roughness must be added to the free-air drag to produce an estimate of the actual drag. When all drag corrections have been referred to the element's profile area, $A_{Di}$ in Eq. (17.1), the corrected drag coefficient for the a shape element may be found from

$$c_D = c_{D\infty} + \Delta c_{DG} + \Delta c_{DI} + \Delta c_{DP} + \Delta c_{DR}. \tag{17.2}$$

The subscript *"G"* denotes ground effect, *"I"* interference effect, "P" a protuberance, and *"R"* refers to extra roughness. The corrections, each beginning with "Δ", increase (usually) the drag from the free-air measurement.

**Flow Regime** The discussion in Chap. 2 pointed out that most of the operation of the solar car will be in turbulent, separated flow with Reynolds numbers in the $0.5(10^6)$–$10^7$ range. In this range the drag coefficient increases slowly with Reynolds number, i.e., essentially the vehicle's speed, as Fig. 2.6 shows. So it is possible to speak, in a shorthand way, of "the" drag coefficient, as if it were a constant. By this is meant the slowly increasing drag coefficient in the characteristic Reynolds number range mentioned above. Note also that the drag coefficients of very blunt

bodies, like the disk shown in Fig. 2.6, are nearly constant once separation occurs and quite insensitive to the flow regime in the boundary layer.

When combining shape elements and applying corrections, as described earlier, we must use data often taken at different Reynolds numbers. So we rely on the insensitivity of the drag coefficient to Reynolds number changes when the flow regime is separated on a small, blunt body, such as a rearview mirror, or turbulent on a more streamlined body, such as a basic body in the shape of an ellipsoid with a large fineness ratio. As their individual drag coefficients are insensitive to Reynolds number, combining these elements produces a vehicle drag coefficient estimate insensitive to Reynolds number and this is what we observe in testing.

**Shape Geometry** Figure 17.2 shows a side and front view of a wheelless, basic-body shape. The length, $L$, and profile area, $A_D$, already defined, are shown. The *camber line* is the mean line of the shape; that is, it passes through the centroid of every cross-section between the nose and tail. The *chord* is the straight line connecting the points where the camber line intersects the boundary at the nose and tail. The *camber*, $b$, is the perpendicular distance between the camber and chord lines at any location along the chord. The *pitch angle*, $\pi$, is the angle between the chord line and the horizontal, positive up. The chord length, $L_C$, and the body length, $L$, are related by $L/L_C = \cos \pi$. The ratio of the minimum ground clearance to the width, $h_{min}/W$, is called the *clearance ratio*. The ratio of the maximum camber to the chord, $b_{max}/c$, is called the *camber ratio*. The ratio of the height of the profile area to the width, $h_D/W$, is called the *aspect ratio*. The ratio of the length to the diameter of a circle of area $A_D$, $L/d$, is called the *fineness ratio*.

**Steps** The drag build-up method may be divided into eight steps.

1. Set the design ambient temperature, pressure, and airspeed relative to the car. Calculate the air density from the ideal gas law.
2. Make at least side- and front-view drawings of the vehicle to scale on cross-hatched paper (see Fig. 9.2).

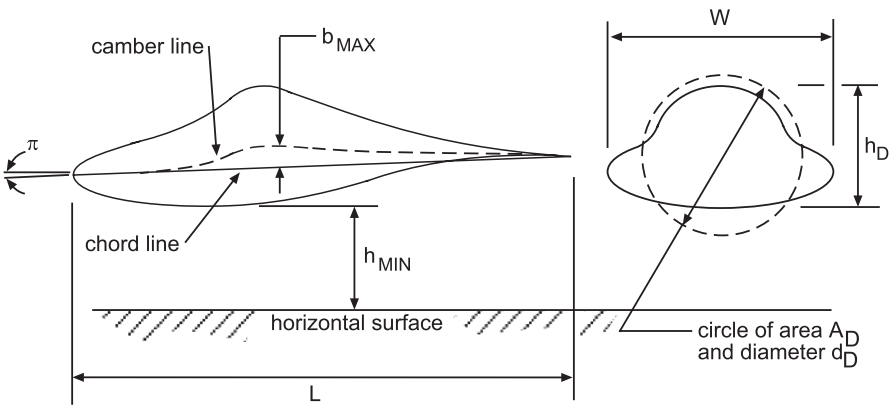


**Fig. 17.2** Shape geometry

3. Divide the car into shape elements for which free-air drag coefficients are available.
4. Calculate the profile area of each shape element and that of the car by counting the scaled squares or partial squares their respective front-view drawings include, allowing for overlap.
5. Estimate the free-air drag coefficient of each shape element for the design conditions and the characteristic length of the shape element.
6. Correct the free-air coefficients for the effects symbolized in Eq. (17.2).
7. Sum the element drag areas as shown in Eq. (17.1) and include the ventilation drag, using the method of Chap. 18 .
8. The drag coefficient is the quotient of the drag area and the vehicle's profile area found in step 4.

Two examples of the application of steps 1 through 8 are presented in Chap. 9. Hoerner (1965) uses this method to predict the drag of an ME-109-G, a German fighter aircraft used in World War II.[1]

## 17.2 Shape Elements

The remainder of this chapter is devoted to presenting free-air drag coefficient information for shape elements and protuberances, and means of correcting for interference and ground effect. Some information is presented as graphs. These were constructed by carefully measuring points from the data in the referenced source and then fitting interpolating curves through these points. Each such curve has a correlation coefficient[2] of at least 0.99. This information is limited to that required for the examples in Chap. 9. However, a very large amount of information is available in the literature. Consult the references at the end of this chapter.

**Ellipsoid** Table 17.1, from White (1986), presents drag coefficient data for ellipsoids of various fineness ratios and circular cross-sections. The data are for both laminar separated flow and turbulent separated flow. The reference area is $\pi d^2/4$. To interpolate in Table 17.1, use $c_D = 0.4311(L/d)^{0.3994}$ for laminar flow and $c_D = 0.1835(L/d)^{-0.4590}$ for turbulent flow.

**Table 17.1** Free-air drag coefficient of ellipsoid ($R_d \geq 10^4$)

| $L/d$ | Laminar | Turbulent |
|---|---|---|
| 0.75 | 0.5 | 0.2 |
| 1 | 0.47 | 0.2 |
| 2 | 0.27 | 0.13 |
| 4 | 0.25 | 0.1 |
| 8 | 0.2 | 0.08 |

[1] Page 14–3

[2] As previously explained: a measure of the goodness of the fit, with 1.0 indicating an exact fit.

**Airfoils** The zero-lift drag coefficient data in Table 17.2 was read from the airfoil section data in Abbott and von Doenhoff (1959) and that in Table 17.3 from Bullivant (1941). "$R_C$" is the Reynolds number based on the section chord. The reference area used to define $c_D$ is the unit planform area, that is, the product of the chord and the unit span. Hence, to convert to a profile area reference,

$$c_{D_{profilearea}} = c_{D_{planformarea}} \frac{c}{t}. \tag{17.3}$$

The tables show both four-digit and six-digit airfoil designations. The meaning of the four- and six-digit designations is given in the next two Tables (17.4 and 17.5).

**Wheels** Adding wheels to a basic body shape can give the largest increase in drag. For example, Morelli (1983) reported a drag coefficient increase of about 0.09 from adding four wheels to a basic body which had an initial drag coefficient of about 0.06. Thus the wheels alone increased the drag by more than the drag of the entire basic body.

A wheel is essentially a short, rotating cylinder. In free air, friction and separation cause drag on the wheel. When the wheel is rolling on the ground, ground interference comes into play. Finally, when the wheel is installed on a car inside a wheel housing, additional effects are induced by the housing and the external flow about the car. Clearly this is in general a complex situation not easily reduced to simple rules.[3]

However, Cogotti (1983) pointed out that according to Morelli (1969), the drag coefficient of an isolated wheel, when based on the profile area of its unshielded

**Table 17.2** Free-air airfoil section drag coefficients (Lift = 0)

| $R_C$ | $3(10^6)$ | $6(10^6)$ | $9(10^6)$ |
|---|---|---|---|
| NACA section | | | |
| 0006 | 0.0043 | 0.0050 | 0.0053 |
| 0009 | 0.0052 | 0.0055 | 0.0055 |
| 0012 | 0.0057 | 0.0057 | 0.0057 |
| 2415 | 0.0070 | 0.0065 | 0.0065 |
| 2418 | 0.0074 | 0.0066 | 0.0065 |
| 2421 | 0.0078 | 0.0070 | 0.0070 |
| 2424 | 0.0087 | 0.0081 | 0.0075 |
| $63_2$–015 | 0.0053 | 0.0051 | 0.0048 |
| $63_3$–018 | 0.0057 | 0.0052 | 0.0049 |
| $63_4$–021 | 0.0064 | 0.0056 | 0.0053 |

**Table 17.3** More free-air airfoil section drag coefficients (Lift = 0)

| $R_C(10^{-6})$ | 1.75 | 2.00 | 2.50 | 3.00 | 4.00 | 5.00 | 6.00 | 7.50 |
|---|---|---|---|---|---|---|---|---|
| NACA section | | | | | | | | |
| 0018 | 0.0080 | 0.0079 | 0.0077 | 0.0076 | 0.0075 | 0.0073 | 0.00715 | 0.0070 |
| 0025 | 0.0089 | 0.0088 | 0.0082 | 0.0081 | 0.0081 | 0.0081 | 0.0081 | 0.0081 |

[3] Fortunately, solar racing cars can take advantage of some options that passenger cars usually cannot. Solar racing cars can use wheels with smaller thickness-to-diameter ratios, and thus smaller drag areas. They can partially enclose the wheels in streamlined fairings or in nearly-sealed wheel housings.

**Table 17.4** NACA four-digit airfoil designation

| Digit | Meaning |
|---|---|
| 1 | Maximum distance of mean line from chord (%*c*) |
| 2 | Distance from leading edge to maximum camber (*c*/10) |
| 3 & 4 | *t*/*c* (%) |

**Table 17.5** NACA six-digit airfoil designation

| Digit | Meaning |
|---|---|
| 1 | Series designation |
| 2 | Position of minimum pressure from leading edge (c/10) |
| 3 | $c_L$ range ± design $c_L$ of low drag (10ths) |
| 4 | Design $c_L$ (10ths) |
| 5 & 6 | t/c (%) |

portion, is approximately unchanged when the wheel is partly enclosed by the fairing. These results suggest the thumb rule that the drag of the wheel is proportional to the profile area of its unshielded portion,

$$A_{DW} = hb_W, \tag{17.4}$$

where, $A_{DW}$ is the unshielded profile area, $h$ is the height of this area above ground, and $b_W$ is the width of the wheel.

Figure 17.3 shows the drag coefficient of an isolated, stationary wheel as a function of yaw angle. Accounting for the forgoing discussion, the drag of a wheel (the jth one) would be

$$D_{W_j} \approx qc_{DW_{isolated}} A_{DW_j}, \tag{17.5}$$

Where, $c_{DW_{isolated}}$would be taken from Fig. 17.3, and $q$ is the dynamic pressure defined in Chap. 2. The equation of the curve in the figure is

$$c_{DW_{isolated}} = 0.5272 - 3.2289(10^{-4})\beta + 4.8399(10^{-4})\beta^2, \tag{17.6}$$

Where, $\beta$ is the yaw angle in degrees. Interpret this as the "free-air" drag coefficient of the wheel.

The airflow changes direction at the front of the car in order to pass around the car. Therefore, the wheel yaw angles will probably differ from zero for vehicles with two wheels in front.[4] Figure 17.3 shows that this will probably cause the drag to increase.[5] The yaw angle will depend upon the direction of the relative wind near the wheels, which will be difficult to estimate.

[4] The flow would be symmetric with respect to a centered single wheel.

[5] The drag coefficient passes through a maximum at $\beta \approx 15^{\circ}$ (not shown).

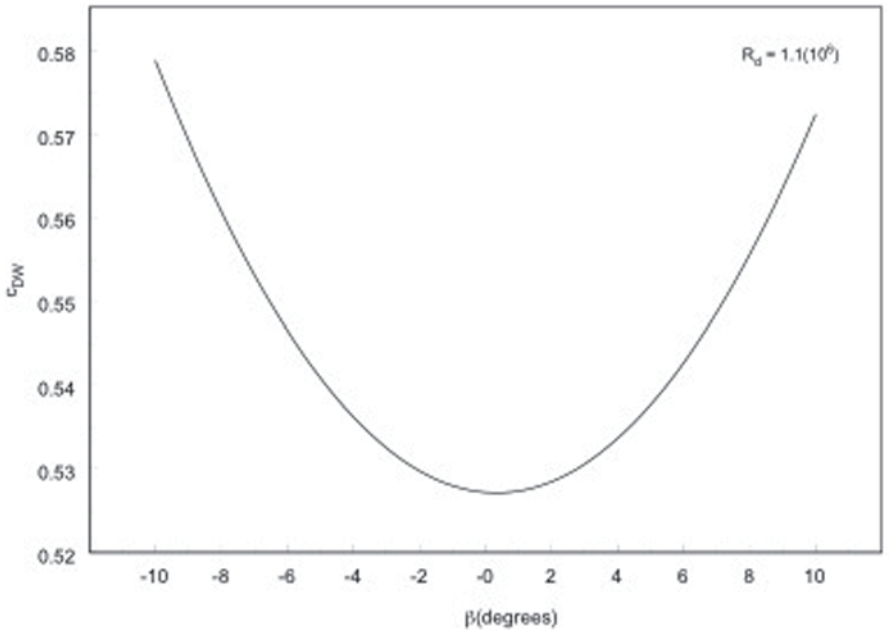


**Fig. 17.3** Drag coefficient of an isolated wheel. (adapted from Cogotti 1983)

Cogotti's data show that the rotation of the wheel may slightly increase or decrease the drag of wheels in housings. Which effect occurs depends upon the inner and outer housing shape and the location of the wheels relative to the front of the car. We will make no attempt to account for wheel rotation.

Cogotti also found that placing a flat or nearly flat fairing over standard wheel rims decreases the drag of the car (not the wheel alone) by an amount

$$\Delta c_{D_{rf}} = -0.009 \pm 0.003. \tag{17.7}$$

The subscript *"rf"* denotes "rim fairing."

**Protuberance** This category includes items such as rearview mirrors and antennas which are small enough not to cause significant interference drag. They can therefore be included using only their free-air drag characteristics. In addition, as Pershing and Maskai (1976) pointed out, their characteristic lengths are small enough to ensure that the flow about the protuberance is in the laminar-separated region. Based on information in Hoerner (1965) the drag coefficients for cylindrical protuberances, such as flat mirrors and antennas, are all about 1.1 and for cup-like shapes which are convex in the upwind direction, are about 0.4.[6]

[6] Pershing and Maskai also point out that such items may be located in regions of accelerated or locally-separated flow. This will change their drag contributions.

## 17.3 Interfering Flows

For most of the plots in this section, the original data has been normalized by the tested $c_{D\infty}$. This helps to minimize dependence on the airfoil shapes tested.

**Parallel Airfoils** Consider the two identical symmetric airfoils used as fairings over the rear wheels of the car in Fig. 17.1. Figure 17.4 shows first the flow around the airfoil shape when tested independently at zero angle of attack to the wind.[7]

There is no lift force on the airfoil because the angle of attack is zero. Thus the free-air drag coefficient could be selected from Tables 17.2 and 17.3. Figure 17.4 shows that free-air drag exists when $y_m/t$ is greater than 5.

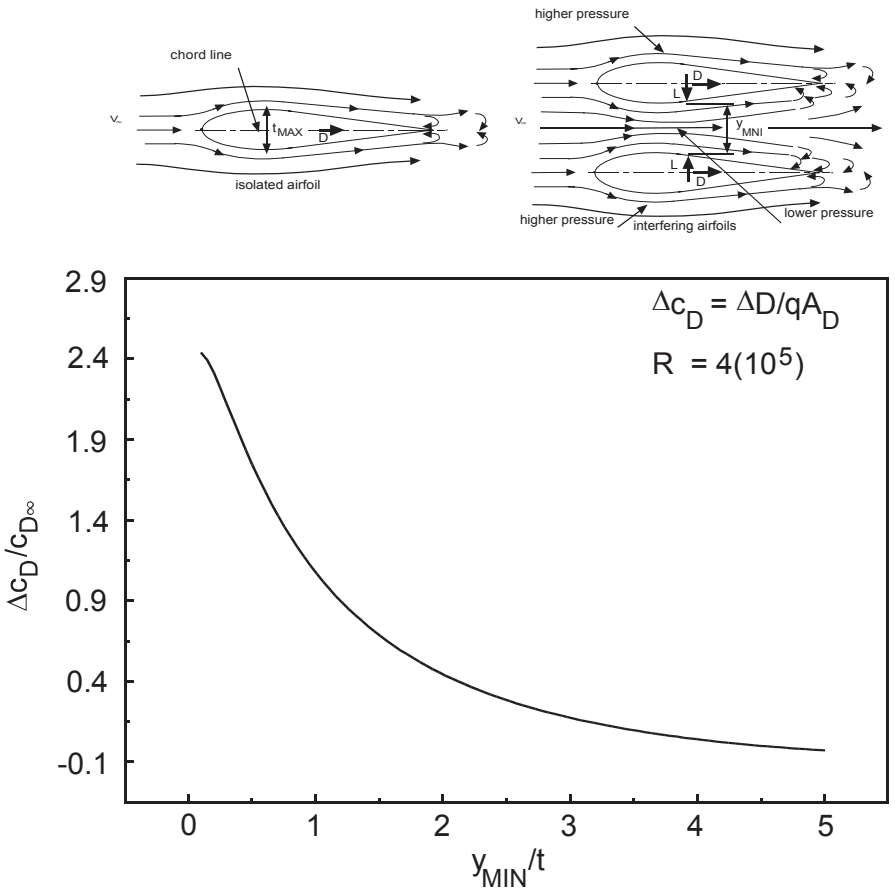


**Fig. 17.4** Interference between parallel airfoils

[7] The angle of attack is the angle between the chord line and the relative wind.

When the airfoils are brought near each other on the car, the symmetry of the flow is disturbed because of the Bernoulli effect (Chap. 2). The figure shows that the lower pressure region created between the fairings by the acceleration of the flow creates an inward-directed "lift" force with an associated increase in drag. The increase in the drag coefficient over the free-air drag has been plotted in Fig. 17.4 as a function of $y_{min}/t$, the minimum spacing divided by the airfoil thickness. The curve was based on the data reported in Biermann and Herrnstein (1933).

$$\frac{\Delta c_{DI}}{c_{D\infty}} = 2.819929 - 2.084828\frac{y_m}{t} + 0.614002\left(\frac{y_m}{t}\right)^2 - 0.084466\left(\frac{y_m}{t}\right)^3 + 0.00450\left(\frac{y_m}{t}\right)^4. \tag{17.8}$$

The interference is zero for $y_{min}/t$ more than about 5.

The drag increase is defined as

$$\Delta D = (D_1 + D_2)_{interfering} - (D_1 + D_2)_{free}. \tag{17.9}$$

In the parallel airfoil case, the symmetry of the geometry implies that $D_1 + D_2 = 2D_1$ or $2D_2$, and that the total profile area will be twice the profile area of one airfoil. Such is not the case for airfoils in tandem.

**Tandem Airfoils** Figure 17.5 shows two identical symmetrical airfoils in tandem. Cogotti also found that placing a flat or nearly flat fairing over standard wheel $x/c$ is greater than 4. The free-air drag coefficients could be selected from Tables 17.2 or 17.3. The upstream and downstream curves are, respectively,

$$\frac{\Delta C_{D_1}}{C_{D\infty}} = 0.000143\exp\left[\begin{array}{l} 26.395047\frac{x}{c} - 24.782729\left(\frac{x}{c}\right)^2 \\ +10.118397\left(\frac{x}{c}\right)^3 - 1.911910\left(\frac{x}{c}\right)^4 + 0.13672\left(\frac{x}{c}\right)^5 \end{array}\right] \cdot \tag{17.10}$$

and

$$\frac{\Delta C_{D_1}}{C_{D\infty}} = 2.630656 - 0.575883\ln\frac{x}{c} + 21.487285\left(\ln\frac{x}{c}\right)^2 - 37.823911\left(\ln\frac{x}{c}\right)^3 + 25.489452\left(\ln\frac{x}{c}\right)^4 - 6.118458\left(\ln\frac{x}{c}\right)^5. \tag{17.11}$$

Hoerner (1965) assumes that the increase in the drag of the rear airfoil is caused by separation induced by the wake of the upstream airfoil. The decrease in the drag of the upstream airfoil is explained by the increased static pressure between the airfoils

when they are close together. Note that these two effects tend to offset one another so that the sum of the interference corrections is approximately zero.

**Airfoil-Wall** Figure 17.6 shows an airfoil attached to a wall. According to Hoerner (1965) the interference drag is

$$\Delta c_{Dt} = \frac{\Delta D_I}{qt^2} = 0.75\left(\frac{t}{c}\right) - \frac{0.0003}{\left(\frac{t}{c}\right)^2}. \tag{17.12}$$

Hoerner writes that this interference drag is independent of the span of the airfoil. Hence, it is referenced to the "thickness area," $t^2$, instead of the profile area. Figure 17.6 shows $\Delta c_{Dt}$ going to zero below a $t/c$ of 0.1. Hoerner points out that the data upon which Eq. (17.12) was based suggests this, but does not actually extend to zero beyond 0.1.

Equation (17.2) requires that $c_{D\infty}$ and corrections to it be referenced to the shape element's drag area. This is $A_D = tS$, where $S$ is the airfoil's span. Using this formula, the reader can show that $\Delta c_{DI} = \frac{\Delta D_I}{qA_D} = c_{Dt}\frac{A_D}{S^2} = c_{Dt}\frac{t}{S}$.

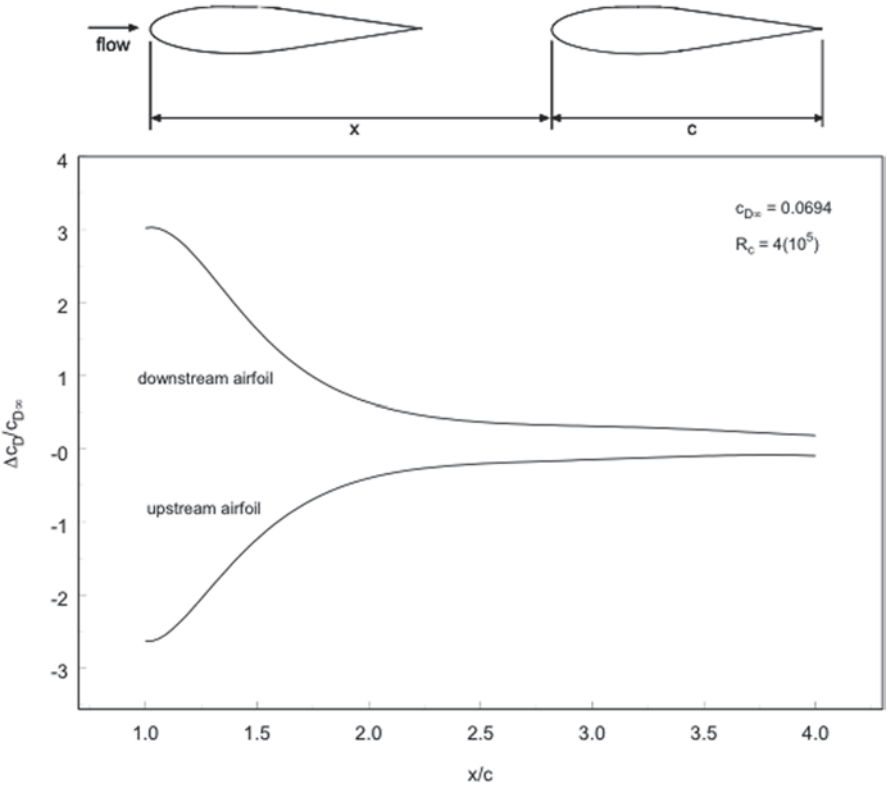


**Fig. 17.5** Interference between tandem airfoils. (Adapted from Bierman and Hermstein 1933)

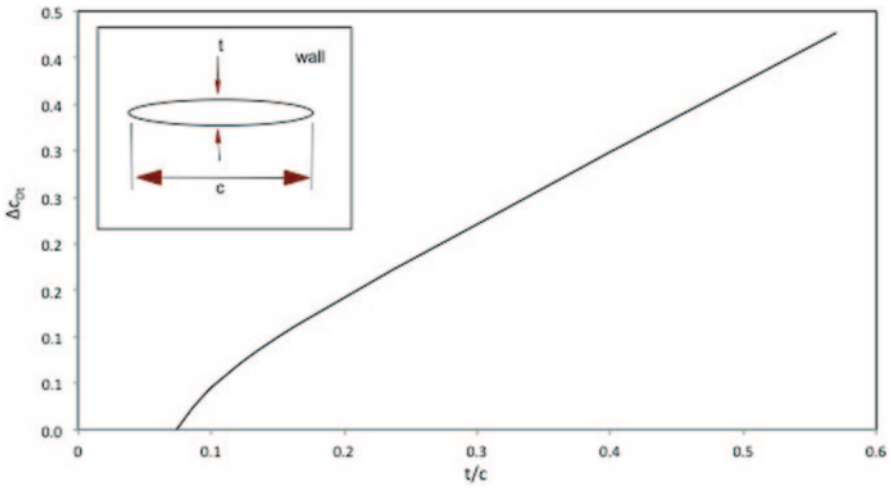


**Fig. 17.6** Airfoil-wall interference

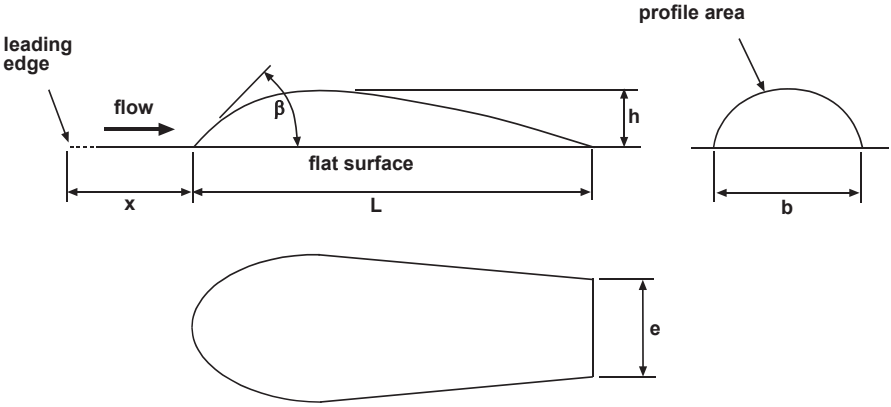


**Fig. 17.7** Canopy dimensions

**Fairing** Figure 17.7 shows a fairing (which could be a canopy) placed on a plane surface. Hoerner (1965) summarizes the results of a number of tests. The drag of the fairing or canopy is a function of its height ratio, $h/x$, and (specially defined) fineness ratio, $L/h$, width ratio, e/b, and the angle, β, between the tangent to its leading edge and the plane wall.

Following Hoerner, we assume a $c_{D\infty}$ of 0.03. As the height ratio becomes less than about 0.3, $\Delta c_{Dl}/c_{D\infty}$ rises, reaching a maximum of about 1.0 at about 0.1. At height ratios larger than 0.3, $\Delta c_{Dl}/c_{D\infty}$ is about zero. All tests that Hoerner summarizes were done at $R_L$ greater than the critical Reynolds number. Hence, he attributes the influence of $h/x$ to be the interference drag associated with junction between the surface and the fairing.

The shape of the canopy, described by $\beta$, $L/h$, and $e/b$, also affects the drag. Although, Hoerner gives no measurements of the tangent angle, he shows that reducing $\beta$ to considerably less than 90 can reduce $\Delta c_{D_I}/c_{D_\infty}$ by as much as 43 %. The effect of increasing $L/h$ is generally to increase the interference drag.

$$\frac{\Delta c_{D_I}}{c_{D_\infty}} = \begin{cases} 0.4, & 5 \le \dfrac{L}{h} \le 15 \\ 0.0667\dfrac{L}{h} - 1, & 15 < \dfrac{L}{h} < 30 \end{cases}. \tag{17.13}$$

## 17.4 Ground Effect

The discussion in Chap. 2 explained that when a shape element is moved toward the ground from free air, lift and drag forces are created by the alteration in the pressure distribution caused by the Bernoulli effect between the element and the ground. This is similar to the parallel airfoil interference effect, with the plane of symmetry between the foils representing the "ground." As we shall presently see, ground effect is dependent upon the shape and pitch angle of the element.

We present curves that have been derived from the results of Morelli (1983). This paper presented data from wind tunnel tests of the lift and drag forces on cambered, wheelless, basic-body shapes (similar in appearance to Fig. 17.2) designed to minimize the drag near the ground by adjusting the camber ratio. Call these "shark" shapes, as in Chap. 9. Three $\Delta c_D/c_{D_\infty}$ curves for these shapes, are plotted in Fig. 17.9. They display $\Delta c_D/c_{D_\infty}$ for zero pitch and camber ratios of 3.7, 5.3, and 6.9 % as a function of clearance ratios from 0.05 to 1.0[8]. Morelli (1983) shows that the zero pitch data approximately represents small pitch angles, say between $\pm 1^\circ$. At larger pitch angle magnitudes the drag coefficient is higher.

Morelli (1983) also displayed $c_D$ data for a family of teardrop shapes of different camber ratios as a function of clearance ratio at zero pitch angle. The results for $\pm 1^o$ pitch were nearly the same. The 0 and 3 % camber ratio curves from this family are also shown in Fig. 17.8. The data were taken at a chord Reynolds number of $4.7(10^6)$.

The free-air drag coefficients of all the shapes are given in the figure.

The curves show the strong effect of clearance ratio on the drag. For the teardrop shapes, as the clearance ratio increases the drag decreases, with the lowest value occurring in free air. However, for the shark shapes at the two higher camber ratios, the drag coefficient passes through a minimum in the clearance ratio range 0.1–0.2, followed by a shallow maximum.

The general form of the equation of the curves for the shark shapes is

$$\frac{\Delta c_{D_G}}{c_{D\infty}} = a_0 + a_1 ln\frac{h_{min}}{W} + a_2\left(ln\frac{h_{min}}{W}\right)^2 + \rightleftharpoons + a_n\left(ln\frac{h_{min}}{W}\right)^n. \tag{17.14}$$

[8] According to Morelli (1983), most automobiles lie between clearance ratios of 0.05 and 0.2.

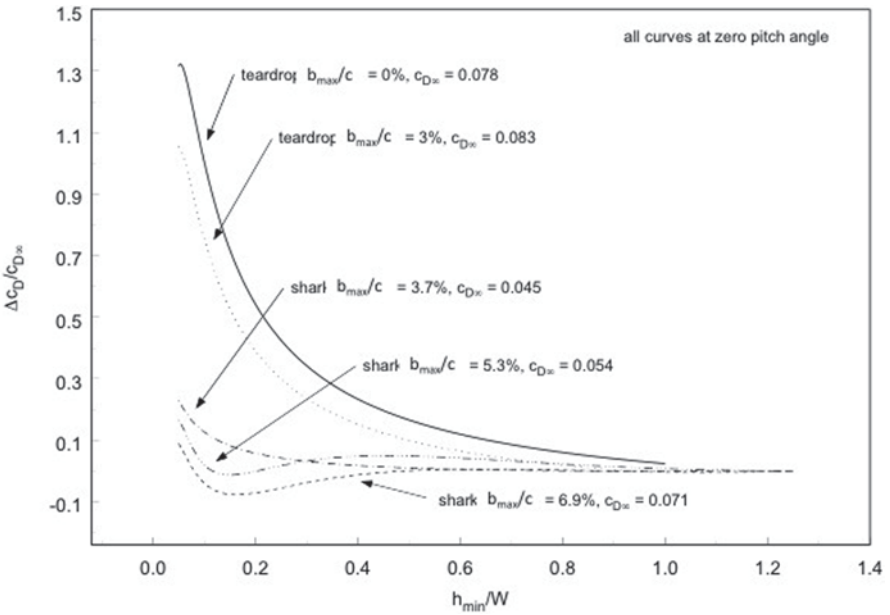


**Fig. 17.8** Ground effect for two shapes. (Adapted from Morelli (1983))

Table 17.6 gives the set of *a*'s for each of these curves.

The equation for the teardrop curves has the form

$$\frac{\Delta c_{D_G}}{c_{D\infty}} = a_0 + a_1\left(\frac{h_{min}}{W}\right)^{-1} + a_2\left(\frac{h_{min}}{W}\right)^{-2}. \tag{17.15}$$

Table 17.7 gives the *a*'s for each teardrop camber ratio case

## 17.5 Flat Plate

The critical Reynolds number for a flat surface with the flow parallel to it is

$$R_{x_c} \approx 5(10^5) - 3(10^6). \tag{17.16}$$

**Table 17.6** Shark shape curve constants

| Camber ratio (%) | $a_o$ | $a_1$ | $a_2$ | $a_3$ | $a_4$ | $a_5$ | $a_6$ |
|---|---|---|---|---|---|---|---|
| 3.7 | 0.00031 | −0.00132 | 0.01741 | −0.00254 | 0 | 0 | 0 |
| 5.3 | 0.00776 | −0.05589 | 0.08372 | 0.12379 | −0.00117 | −0.02897 | −0.00599 |
| 6.9 | −0.0041 | −0.0069 | −0.0928 | 0.2371 | 0.1303 | 0.0203 | 0 |

**Table 17.7** Teardrop shape curve constants

| Camber ratio (%) | $a_0$ | $a_1$ | $a_2$ |
|---|---|---|---|
| 0 | −0.1256 | 0.1541 | −0.0041 |
| 3 | −0.1218 | 0.1168 | −0.0029 |

The upper limit corresponds to a very smooth plate. The symbol *"$x_c$"* is the distance from the leading edge of the plate to the flow transition. The friction drag coefficient is defined as

$$c_{DF} = \frac{D_F}{qA_W}, \tag{17.17}$$

where, $A_W$ is the wetted area of the surface and the subscript *"F"* denotes "friction." The following expression gives the friction drag coefficient of one side of the plate when the laminar—turbulent transition occurs on the plate and the width of the transition region in the flow direction is ignored.[9]

$$c_{DF} = \frac{1.328}{R_{x_x}^{\frac{1}{2}}}\frac{x_c}{L} + \frac{0.031}{R_L^{\frac{1}{7}}}\left[1-\left(\frac{x_c}{L}\right)^{\frac{7}{8}}\right]. \tag{17.18}$$

Bear in mind that Eq. (17.18) applies to flow over a smooth plate.

## 17.6 Roughening

Joints occur around access doors or around other portions of the body that must be repositioned. There may be isolated defects such as cracks or pits, or there may be wires and fasteners that project into the airflow. The distinguishing parameters differ in each case. Hoerner (1965) contains methods for accounting for many of these relatively isolated defects.

Now, suppose the roughness is approximately uniformly distributed over the surface. Then it makes sense to characterize the smoothness of the surface by the ratio $L/\varepsilon$, where $\varepsilon$(Greek "epsilon") is the mean roughness height. The larger this *relative roughness*, the smoother the surface is relative to its length. For example, the 800-odd cells of the solar array are often applied directly to the array substrate and thus are raised above it by perhaps 1–2 mm. In addition, there may be 1.0 mm thermal expansion gaps left between the cells. If the glazing does not smooth the array sufficiently, the cells will contribute additional surface roughening which could be characterized by a relative roughness.

[9] $D_F$ was calculated over the laminar and turbulent regions (x = 0 to $x_C$ and $x_C$ to L, respectively). The results were added and (17.17) applied.

We will consider the flat surface of the previous section. (The surface of an actual vehicle will be curved. But for practicality we will ignore this when considering roughness as long as we judge that the flow is strongly one-dimensional.) Suppose the flow is turbulent over the entire surface ($x_c = 0$ in Eq. (17.18)). If the Reynolds number continues to increase, the flow will enter the *fully rough* regime. Then the friction drag coefficient no longer depends upon the Reynolds number, but only on the relative roughness. Also, the Reynolds number at which this condition occurs becomes smaller as the relative roughness is reduced. If we were to measure the friction drag coefficient on a smooth surface, $L/\varepsilon$ about $10^6$ perhaps, in laminar flow at a Reynolds number of $5(10^5)$, we would find a value of about 0.002. Suppose we were to paint that surface with a roughening agent that reduced $L/\varepsilon$ to 500. At the same Reynolds number the flow would move into the fully rough regime and the friction drag coefficient would rise to 0.01, a 5-fold increase.

The *critical relative roughness* is that which precipitates fully rough flow. From information in White (1986),

$$\left(\frac{L}{\varepsilon}\right)_c = -654963 + 335446.3 log R_L - 57477.5(log R_L)^2 + 3299.78(log R_L)^3. \quad (17.19)$$

## 17.7 Other Methods

**Drag Rating** White (1967) presented a method in which features of vehicles were assigned to nine categories and then awarded a score, with the lowest score (one) assigned to the feature contributing the least to the drag. The sum of the category ratings is the drag rating, $R$, of the vehicle. The method does not incorporate ventilation drag or ground and pitch angle effects. The correlation relating the drag rating to the drag coefficient is

$$c_D = 0.16 + 0.0095R. \quad (17.20)$$

This relation was developed from drag data for 141 vehicles and it correlates that data is within ±7%.

Note that even if a vehicle received a drag rating of zero, Eq. (17.20) would predict a drag coefficient of 0.16, higher than most solar racing cars. However, the method would be useful in the initial stages of design when selecting shape elements, or when modifying a stock body to reduce its drag.

**Feature Build-up** Pershing and Masaki (1976) reported a method that is well adapted to predicting the drag of automobile shapes similar to that of the typical sedan. Equations for the drag contribution of the elements of the body's shape were developed from the available test data. These equations were in terms of the details of the shape element. For example, the front hood drag coefficient is to be calculated from

$$c_{D_{hood}} = 0.707 \frac{\left(\frac{A_h - A_F}{L_h}\right)^2}{A_R}. \tag{17.21}$$

$A_h$ is the projected area of the body below the hood-windshield intersection, $L_h$ is the length of the hood, $A_F$ is the front end projected area, and $A_R$ is the projected area of the car (less protuberances). If the difference $A_h$—$A_F$ is negative, it is to be set to zero.

The method does not account for the effects of lift, side wind, and ground clearance, and it assumes a fixed wheel drag coefficient of 0.14. It accounts for ventilation drag.

Smalley and Lee (1978), reported that this method agreed with wind tunnel data to within ± 10 % for 13 of 17 vehicle tests. Five of which were duplicate tests using a different tunnel blockage correction method. Three of the outliers were 12–18 % below the tunnel tests and one was 16.5 % higher.

Due to its correlation with details of the vehicle's design, this method will be very useful for setting shape details, that is, actual dimensions rather than qualitative features, when starting with stock bodies. Its major drawback is the use of a large, constant, wheel drag coefficient. As in the drag rating method case, this value alone is larger than the drag coefficient of most solar racing cars.

Ashley and Carr (1982); Rose (1986); and Calkins and Chan (1998) have further developed the feature build-up method. Calkins and Chan have incorporated a refined version of the method in a drag prediction tool called CDaero. CDaero is a component of the Automobile Design Support System reported by Calkins et al. (1996). The refined feature build-up method estimates the drag of the wheels from their exposed projected area, as in this chapter, instead of assuming a constant value. The calculation is for zero yaw and does not account for ground effect.

## References

Abbott, I. H., & von Doenhoff, A. E. (1959). *Theory of wing sections*. New York: Dover Publications, Inc..

Ashley, C., & Carr, G. (1982). A Prediction Method for the Aerodynamic Drag of Cars, *Energy and Mobility: XIX International FISITA Congress Proc., Melbourne, Australia, Nov. 8–12, 1982*, SAE paper 82068, Parkville, Victoria, Australasia.

Biermann, D., & Herrnstein, Jr., W. H. (1933). Interference Between Struts in Combinations, NACA-TR-468.

Bullivant, W. K. (1941). Tests of the NACA 0025 and 0035 Airfoils in the Full-Scale Wind Tunnel, NACA-TR-708.

Calkins, D. E., & Chan, W. T. (1998). 'CDaero'-A Parametric Aerodynamic Drag Prediction Tool, *Developments in Vehicle Aerodynamics (SP-1318), International Congress and Exposition, Detroit, Michigan, February 23–26*, *1998*, SAE paper 980398, SAE Warrendale, PA.

Calkins, D. E., Guan, L., & Koeser, L. (1996). Automobile Conceptual Design Support System (AutoDSS), SAE paper 960551, *Proc. SAE International Congress and Exposition, Detroit, Michigan, 26–29 February*, *1996*, SAE Warrendale, PA.

Cogotti, A. (1983). Aerodynamics of Car Wheels, *Int. J. of Vehicle Design*, Technological Advances in Vehicle Design Series, SP3, *Impact of Aerodynamics on Vehicle Design*, Dorgham, M. A. ed., Interscience Enterprises Ltd., La Motte Chambers, United Kingdom, pp. 173–196.

Hoerner, S. F. (1965). *Fluid-Dynamic Drag*, Hoerner Fluid Dynamics. Bakersfield.

Kurtz, D. W. (1979). *Aerodynamic Characteristics of Sixteen Electric, Hybrid, and Subcompact Vehicles, Complete Data*, JPL Publication 79–59, (NASA-CR-158814 and NTIS N79-29107), Jet Propulsion Laboratory, Pasadena, California.

Kurtz, D. W. (1980). *Aerodynamic Design of Electric and Hybrid Vehicles: A Guidebook*, JPL Publication 80–69 (NASA-CR-163744 and NTIS N81-12943), Jet Propulsion Laboratory, Pasadena, California.

Morelli, A. (1983). Aerodynamic Basic Bodies Suitable for Automobile Applications, *Int. J. of Vehicle Design*, Technological Advances in Vehicle Design Series, SP3, *Impact of Aerodynamics on Vehicle Design*, Dorgham, M. A. ed., Interscience Enterprises Ltd., La Motte Chambers, United Kingdom, pp. 70–98.

Pershing, B., & Masaki, M. (1976). Estimation of Vehicle Aerodynamic Drag, *EPA-460/3-76-025 (NTIS PB 275 948)*, National Technical Information Service, Washington, DC.

Rose, M. J. (1986). Appraisal and Modification of the Empirical Method for Predicting the Aerodynamic Drag of Cars, report no. 1986/1, Motor Industry Research Association (MIRA), England.

Schlichting, H. (1979). *Boundary-layer theory* (7th ed.). New York: McGraw-Hill Book Company.

Smalley, W. M., & Lee, W. B. (1978). *Assessment of an Empirical Technique for estimating Vehicle Aerodynamic Drag from Vehicle Shape Parameters*, Aerospace Corporation, El Segundo, CA, NTIS accession number PB-292 160/9, NTIS issue number 7913.

White, R. G. S. (1967). A Rating Method for Assessing Vehicle Aerodynamic Drag Coefficients, Motor Industry Research Association, United Kingdom.

White, F. M. (1986). *Fluid mechanics* (2nd ed.). New York: McGraw-Hill Book Company.